HHS Public Access

Author manuscript

Int J Pharm. Author manuscript; available in PMC 2017 October 15.

Published in final edited form as:

Int J Pharm. 2016 October 15; 512(1): 305–313. doi:10.1016/j.ijpharm.2016.08.047.

Nanocomposite Microparticles (nCmP) for the Delivery of Tacrolimus in the Treatment of Pulmonary Arterial Hypertension

Zimeng Wang[1], **Julie L. Cuddigan**[1], **Sweta K. Gupta**[1], and **Samantha A. Meenach**[1,2]

[1]University of Rhode Island, College of Engineering, Department of Chemical Engineering, Kingston, RI 02881, USA

[2]University of Rhode Island, College of Pharmacy, Department of Biomedical and Pharmaceutical Sciences, Kingston, RI 02881, USA

Abstract

Tacrolimus (TAC) has exhibited promising therapeutic potential in the treatment of pulmonary arterial hypertension (PAH); however, its application is prevented by its poor solubility, instability, poor bioavailability, and negative systemic side effects. To overcome the obstacles of using TAC for the treatment of PAH, we developed nanocomposite microparticles (nCmP) for the pulmonary delivery of tacrolimus in the form of dry powder aerosols. These particles can provide targeted pulmonary delivery, improved solubility of tacrolimus, the potential of penetration through mucus barrier, and controlled drug release. In this system, tacrolimus-loaded polymeric nanoparticles (NP) were prepared via emulsion solvent evaporation and nCmP were prepared by spray drying these NP with mannitol.

The NP were approximately 200 nm in diameter with narrow size distribution both before loading into and after redispersion from nCmP. The NP exhibited smooth, spherical morphology and the nCmP were raisin-like spheres. High encapsulation efficacy was achieved both in the encapsulation of tacrolimus in NP and that of NP in nCmP. nCmP exhibited desirable aerosol dispersion properties, allowing them to deposit into the deep lung regions for effective drug delivery. A549 cells were used as *in vitro* models to demonstrate the non-cytotoxicity of TAC nCmP. Overall, the designed nCmP have the potential to aid in the delivery of tacrolimus for the treatment of PAH.

Graphical abstract

Corresponding Author: Samantha A. Meenach, University of Rhode Island, 205 Crawford Hall, 16 Greenhouse Road, Kingston, RI, 02881, USA. smeenach@uri.edu.

AUTHOR DISCLOSURE STATEMENT

No conflicts of interest exist.

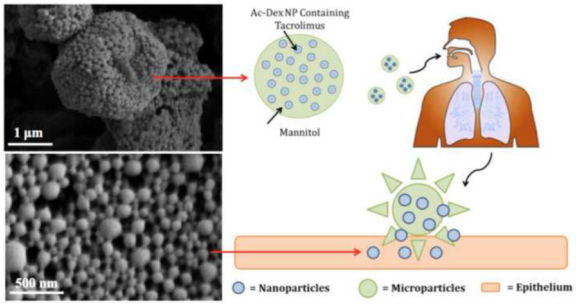

Keywords

Nanocomposite microparticles; pulmonary delivery; pulmonary arterial hypertension; spray drying; tacrolimus

1. INTRODUCTION

Pulmonary arterial hypertension (PAH) is a progressive cardiovascular disease that results in limited exercise capacity, right ventricular heart failure, and ultimately death (1). It is hemodynamically defined as an increased mean pulmonary arterial pressure higher than 25 mmHg with a pulmonary capillary wedge pressure lower than 15 mmHg at rest (2, 3). Patients often develop PAH because of genetic and/or environmental insult, resulting in endothelial cell apoptosis, loss of distal vessels, and occlusive vascular remodeling, which causes elevated pulmonary arterial pressures.

The primary treatment options currently available for patients with PAH are based on drugs with vasodilatory properties that improve cardiopulmonary function. Unfortunately, these drugs show no effect on prohibiting the progress of or improving obliterative vascular pathology. Because of this, the only option for many patients to improve their health and quality of life is heart-lung transplantation. Therefore, new approaches to utilize compounds that focus on activating cellular mechanisms to reverse vascular remodeling are under investigation (4). Improving the function of the bone morphogenetic protein receptor-2 (BMPR2) signaling pathway is a potential direction in the development of improved PAH therapies, as the mutations of BMPR2 have been identified as a cause of inherited PAH, accounting for 60 to 80% of familial cases. BMPR2 mutations are also the main cause of 10 to 25% cases in sporadic PAH and 9% of PAH associated with fenfluramine use (4–8).

Since challenges exist in the clinical application of BMPR2 gene therapy, tacrolimus can be applied instead, as it increases signaling of the BMPR2 pathway. Tacrolimus (TAC) is an FDA-approved immunosuppressive drug with a known pharmacokinetic and toxicity profile. Aerosolized tacrolimus has been studied in a few select applications, including to reduce lung transplant rejection (9), airway grafts (10), and to modulate idiopathic pulmonary fibrosis (11). Previous research on the use of TAC to treat PAH has shown that: 1) low-dose TAC can reverse dysfunctional BMPR2 signaling in pulmonary artery endothelial cells (ECs) from patients with idiopathic PAH, 2) low-dose TAC can prevent exaggerated chronic hypoxic PAH in mice with conditional BMPR2 deletion in ECs, and 3) low-dose TAC can

reverse severe PAH in rats with medial hypertrophy following monocrotaline exposure and in rats with neointima formation following vascular endothelial growth factor receptor blockade and chronic hypoxia (4).

Although TAC shows promising potential in the treatment of PAH, its application is hindered by its poor solubility in water (1.3 μg/mL), instability, and limited bioavailability (12–14). In addition to these limiting pharmacokinetic properties, systemic side effects such as neurotoxicity and nephrotoxicity also complicate the clinical use of TAC (15). To overcome this problem, biodegradable polymeric acetalated dextran (Ac-Dex) nanoparticles (NP) can be applied to more safely and effectively deliver TAC. Ac-Dex NP can improve hydrophobic agent solubility, promote drug penetration to obtain higher plasma concentration, provide sustained drug release, and provide reduced systemic side effects due to localized delivery to the lungs.

Ac-Dex is an acid-sensitive, biodegradable, biocompatible polymer that can be prepared in a one-step reaction by reversibly modifying dextran with acetal groups (16). This modification reverses the solubility properties of dextran from hydrophilic to hydrophobic, making it possible to form polymeric particles using standard emulsion or nanoprecipitation techniques. In contrast to poly(lactic-co-glycolic acid) (PLGA) and other polyesters, which are widely applied as excipients in drug delivery applications, Ac-Dex offers several advantages. Most notably, the degradation rate of Ac-Dex can be tuned from minutes to months to suit various applications. Tunable degradation rates are a result in the adjustment of the ratio of cyclic acetal groups with a slower degradation rate to acyclic acetal groups with a faster degradation rate, which can be easily completed by controlling the reaction time during Ac-Dex synthesis. Furthermore, Ac-Dex particulates typically show minimal burst release at physiological conditions (pH 7.4), which is desirable to maintain a steady drug level in the body. Finally, Ac-Dex degrades into the biocompatible, biodegradable, FDA-approved by-products of dextran and very low levels of methanol and acetone (16–19).

Pulmonary aerosols have attracted increasing attention for the treatment of lung diseases, as they are capable of delivering a wide range of therapeutics directly and efficiently to the lungs. Pulmonary delivery systems offer several advantages including increased local drug concentration in the lungs, reduced systemic side effects, rapid onset of action due to the enormous surface area and plentiful capillary vessels in the lung, and avoidance of the first-pass metabolism associated with the liver (20–25). While dry powder aerosolized nanoparticles (less than 500 nm) will be exhaled owing to their small size and mass, aerosolized particles with aerodynamic diameters of 1–5 μm (or larger) can effectively deposit into the lungs. However, this size range is also the size at which particles are commonly phagocytosed by alveolar macrophages, which limits their efficacy as aerosol drug delivery vehicles (26). To overcome these aforementioned obstacles for pulmonary TAC delivery, we developed nanocomposite microparticles (nCmP) in the form of dry powder aerosols (Figure 1). This system is comprised of TAC-loaded Ac-Dex NP entrapped in microparticle carriers with the excipient mannitol. Once the nCmP impact on the surface of the lungs, NP are released to allow for the delivery of TAC.

Mannitol was used as the excipient in the nCmP due to its beneficial properties in aerosol formulations. First, mannitol is highly water-soluble, which ensures rapid decomposition of nCmP in the aqueous environment of mucus and pulmonary surfactant in the lungs, leading to quick release of NP from the nCmP system. Furthermore, mannitol is able to enhance mucus penetration of nanoparticles by increasing fluidity of mucus in the lung (27). Finally, mannitol has been extensively studied as a carrier in spray-dried powder aerosols for pulmonary drug administration and the resulting particles have been shown to exhibit desirable water content, size, and surface morphology for successful aerosol delivery (28–33).

In the present nCmP system, the drug-loaded nanoparticles contain TAC as a therapeutic and these NP are coated by polyvinyl alcohol (PVA). Upon pulmonary administration, the nCmP will deposit on the mucus in the respiratory tract, decompose into free NP and mannitol, and allow the nanoparticles to penetrate the mucus barrier and then release drug to the targeted site. The goal of the described research was the initial development and physicochemical and *in vitro* characterization of the nCmP systems with ability of targeted delivery, improved drug solubility, and potential of efficient penetration of mucus barrier and of controlled release via particle engineering.

2. MATERIALS AND METHODS

2.1 Materials

Dextran from Leuconostoc mesenteroides (9000–11000 MW), pyridinium p-toluenesulfonate (PPTS, 98%), D-mannitol (≥ 98%), 2-methoxypropene (2-MOP, 97%), triethylamine (TEA, ≥ 99%), anhydrous dimethyl sulfoxide (DMSO, ≥ 99.9%), poly(vinyl alcohol) (PVA, MW 13,000–23,000, 87–89% hydrolyzed), dichloromethane (DCM, anhydrous, ≥ 99.8%), deuterium chloride (DCl, 35 weight % in D_2O, 99 atom % D), Tween® 80, potassium phosphate dibasic, potassium phosphate monobasic, and acetonitrile (HPLC grade, ≥ 99.9%) were obtained from Sigma–Aldrich (St. Louis, MO). Deuterium oxide (D_2O, 99.8% atom D) was obtained from Acros Organics (Geel, Belgium). Phosphate buffered saline (PBS), phosphoric acid (extra pure, 85% solution in water), and sodium pyruvate were obtained from Fisher Scientific (Somerville, NJ). Hydranal® KF reagent was obtained from Fluka Analytical. Tacrolimus (FK-506) was purchased from LC Laboratories (Woburn, MA). A549 cells were obtained from American Type Culture Collection (Manassas, VA, USA). Dulbecco's Modified Eagle Medium (DMEM), pen-strep, and Fungizone® were obtained from Life Technologies (Norwalk, CT, USA). Fetal bovine serum (FBS) was obtained from Atlanta Biologics (Flowery Branch, GA, USA) and resazurin was obtained from Acros Organics.

2.2 Methods

2.2.1 Synthesis and NMR Analysis of Acetalated Dextran (Ac-Dex)—Ac-Dex was synthesized as described previously (17) with minor modifications. Briefly, 1 g of lyophilized dextran and 25 mg of PPTS were dissolved in 10 mL anhydrous DMSO. The resulting solution was reacted with 5 mL of 2-MOP under nitrogen gas for 5 minutes and was quenched with 1 mL of TEA. The reaction mixture was then precipitated in basic water

(water and TEA, pH 9), vacuum filtered, and lyophilized (−50 °C, 0.023 mbar) for 24 hours to yield a solid product.

The cyclic-to-acyclic (CAC) ratio of acetal coverage and degrees of total acetal coverage per 100 glucose molecules was confirmed by ^{1}H NMR spectroscopy (Bruker 300 MHz NMR, MA). 10 mg of Ac-Dex was added to 700 μL of D_2O and was hydrolyzed with 30 μL of DCl prior to analysis. The hydrolysis of one cyclic acetal group produces one acetone whereas one acyclic acetal produces one acetone and one methanol. Consequently, from the normalized integrations of peaks related to acetone, methanol, and the carbon ring of dextran, the CAC ratio of acetal coverage and degrees of total acetal coverage per 100 glucoses was determined.

2.2.2 Formation of TAC-Loaded Ac-Dex Nanoparticles (TAC NP)—Tacrolimus-loaded nanoparticles (TAC NP) were prepared via oil/water emulsion and solvent evaporation. 90 mg of Ac-Dex and 10 mg of TAC (10 weight % initial loading) were dissolved in 1 mL of DCM over an ice bath, establishing the organic phase. 3% PVA in PBS, the aqueous phase, was added to the organic phase and the resulting solution was sonicated (Q500 Sonicator, Qsonica, Newtown, CT) for 30 seconds with a 1 second on/off pulse at 70% amplitude. The emulsion was transferred to a spinning solution of 0.3% PVA in PBS and stirred for 4 hours to allow for evaporation of the organic solvent and particle hardening. The solution was then centrifuged at 14000 rpm for 20 minutes to collect the nanoparticles. Nanoparticles were washed once with basic water, redispersed in 0.1% PVA, and lyophilized (−50 °C, 0.023 mbar) for 48 hours.

2.2.3 Formulation of Nanocomposite Microparticles (nCmP) Via Spray Drying —Nanocomposite microparticles (nCmP) were prepared via the spray drying of TAC NP suspensions and mannitol in an aqueous solution using a Büchi B-290 spray dryer (Büchi Labortechnik, AG, Switzerland) in open mode. The spray drying conditions were as follows: 1:1 (weight) ratio of TAC NP to mannitol in DI water, feed solution concentration of 1% (w/v), 0.7 mm nozzle diameter, atomization gas flow rate of 414 L/h using UHP dry nitrogen, aspiration rate of 28 m^3/h, inlet temperature of 50 °C, pump rate of 0.6 mL/min, and nozzle cleaner rate of 4. The resulting nCmP were separated in a high-performance cyclone, collected in a sample collector, and stored in amber glass vials in desiccators at −20 °C.

2.2.4 Particle Morphology and Shape Analysis via Scanning Electron Microscopy (SEM)—The shape and surface morphology of the NP and nCmP were evaluated by SEM using a Zeiss SIGMA VP Field Emission-Scanning Electron Microscope (Germany). nCmP samples were placed on aluminum SEM stubs with double-sided adhesive carbon tabs. Nanoparticles were dispersed in basic water (pH = 9, 10 mg/mL) and this suspension was dropped onto aluminum SEM stubs and then dried at room temperature. Both the NP and nCmP samples were coated with a thin film of a gold/palladium alloy using a BIO-RAD sputter coating system at 20 μA for 60 seconds under argon gas. Images were captured at 5 kV at various magnifications.

2.2.5 Particle Size, Size Distribution, and Zeta Potential Analysis—The size, size distribution, and zeta potential of the NP systems were measured by dynamic light scattering (DLS) using a Malvern Nano Zetasizer (Malvern Instruments, Worcestershire, UK). The NP were dispersed in basic water (pH = 9, 0.3 mg/mL). All experiments were performed in triplicate with a scattering angle of 173° at 25 °C. The mean size (geometric diameter) of the nCmP was measured digitally from SEM images using ImageJ software (Systat, San Jose, CA, USA). Representative micrographs (5000× magnification) for each sample were analyzed by measuring the diameter of at least 100 particles.

2.2.6 Analysis of Nanoparticle Drug Loading and Nanoparticle Loading in nCmP—Drug loading and encapsulation efficacy (EE) of TAC NP and nCmP were determined via Ultra Performance Liquid Chromatography (UPLC, LaChrom, Hitachi, Japan). Detection of TAC was performed using following conditions: C_{18}, 5 μm × 150 mm × 4.6 mm column (Ascentis, Sigma-Aldrich, St. Louis, MO), 1 mL/min pump rate, 6 minute retention time, mobile phase of 70% acetonitrile and 30% phosphoric acid aqueous solution (0.1%), absorbance of 215 nm, and temperature of 50 °C. Drug-loaded NP and nCmP were fully dissolved in the mobile phase prior to analysis. The drug concentration in each sample was quantified by comparison with a standard curve of TAC in its mobile phase. The TAC loading of NP, TAC loading of nCmP, NP loading in nCmP, and TAC EE of NP and nCmP were determined by the following equations:

$$\text{Drug loading} = \frac{\text{mass of drug loaded in NP}}{\text{mass of NP}} \times 100\%$$

$$\text{Drug encapsulation efficacy (EE)} = \frac{\text{mass of drug loaded in NP}}{\text{initial mass of drug in NP formulation}} \times 100\%$$

$$\text{Nanoparticles loading} = \frac{\text{mass of NP loaded in nCmP}}{\text{mass of nCmP}} \times 100\%$$

$$\text{NP loading efficacy} = \frac{\text{mass of NP loaded in nCmP}}{\text{initial mass of NP in nCmP formulation}} \times 100\%$$

2.2.7 *In Vitro* Drug Release from Nanoparticles—The *in vitro* release profiles of TAC from nanoparticles were determined via the release of NP (1 mg/mL, 1.5ml) in modified phosphate buffer (PBS, 0.1 M, pH = 7.4) with 0.5% (w/v) Tween® 80. The NP suspension was incubated at 37 °C and 100 rpm. At various time points NP samples were centrifuged at 14000 rpm for 5 minutes at 4 °C to isolate the NP. 200 μL of supernatant was withdrawn and replaced by the same amount of fresh modified PB in each sample. The withdrawn solutions were analyzed for drug content via UPLC using the same method described previously.

2.2.8 Karl Fischer Coulemetric Titration—The water content of the nCmP was quantified by Karl Fischer (KF) titration using a 737 KF coulometer (Metrohm, Riverview, FL). 10 mg of powder was dissolved in anhydrous methanol. The resulting solution was injected into the KF reaction cell filled with Hydranal® KF reagent and then the amount of water was analyzed accordingly.

2.2.9 Differential Scanning Calorimetry (DSC)—The thermal phase transitions of the nCmP, NP, and their raw components were determined via DSC using a TA Q10 DSC system (TA Instruments, New Castle, DE) equipped with an automated computer-controlled TA instruments DSC refrigerated cooling system. 1 – 3 mg of sample was weighed into Tzero™ alodined aluminum pans that were hermetically sealed. The sealed pans were placed into the DSC furnace along with an empty sealed reference pan. The heating range used was 0 – 200 °C at a heating rate of 10 °C/min.

2.2.10 Powder X-Ray Diffraction (PXRD)—Crystalline states of the nCmP and its raw components were examined by powder X-ray detection (PXRD) using a Rigaku Multiflex X-ray diffractometer (The Woodlands, TX) with a Cu Kα radiation source (40 kV, 44 mA). The samples were placed on a horizontal quartz glass sample holder (3 mm). The scan range was 5 – 60° in 2Θ with a step width of 0.1 and scan rate of 1 °/min.

2.2.11 *In Vitro* Aerosol Dispersion Performance with the Next Generation Impactor (NGI)—*In vitro* aerosol dispersion performance of the nCmP was evaluated using a Next Generation Impactor™ (NGI™, MSP Corporation, Shoreview, MN) equipped with a stainless steel induction port (USP throat adaptor) attachment and stainless steel gravimetric insert cups. The NGI™ was coupled with a Copley TPK 2000 critical flow controller, which was connected to a Copley HCP5 vacuum pump (Copley Scientific, United Kingdom). The airflow rate (Q) was measured and adjusted to 60 L/min in order to model the flow rate in a healthy adult lung before each experiment. Glass fiber filters (55 mm, Type A/E, Pall Life Sciences, PA) were placed in the gravimetric insert cups for stages 1 through 7 to minimize bounce or re-entrapment (34) and these filters were weighed before and after the experiment to determine the particle mass deposited on each stage. Approximately 10 mg of powder was loaded into a hydroxypropyl methylcellulose (HPMC, size 3, Quali-V®, Qualicaps® Inc., Whitsett, NC) capsule and the capsule was placed into a human dry powder inhaler device (HandiHaler, Boehringer Ingelheim Pharmaceuticals, CT) attached to a customized rubber mouthpiece connected to the NGI™. Three HPMC capsules were loaded and released in each measurement and experiments were performed in triplicate. The NGI™ was run with a delay time of 10 s and running time of 10 s. For Q = 60 L/min, the effective cutoff diameters for each stage of the impactor were given from the manufacturer as: stage 1 (8.06 μm); stage 2 (4.46 μm); stage 3 (2.82 μm); stage 4 (1.66 μm); stage 5 (0.94 μm); stage 6 (0.55 μm); and stage 7 (0.34 μm). The fine particle dose (FPD), fine particle fraction (FPF), respirable fraction (RF), and emitted dose (ED) were calculated as follows:

$$\text{Fine particles dose (FPD)} = \text{mass of particles on stages 2 through 7}$$

$$\text{Fine particles fraction (FPF)} = \frac{\text{fine particles dose}}{\text{initial particle mass loaded into capsules}} \times 100\%$$

$$\text{Respirable fraction (RF)} = \frac{\text{mass of particles on Stages 2 through 7}}{\text{total particle mass on all stages}} \times 100\%$$

$$\text{Emitted dose (ED)} = \frac{\text{initial mass in capsules} - \text{final mass remaining in capsules}}{\text{initial mass in capsules}} \times 100\%$$

The experimental mass median aerodynamic diameter ($MMAD_E$) and geometric standard deviation (GSD) for the particles were determined using a Mathematica® program written by Dr. Warren Finlay (34, 35).

2.2.12 Tapped Density and Theoretical Aerodynamic Diameter Analysis—The density of the nCmP was evaluated via tapped density measurements as described previously with minor modifications (36). 30 – 35 mg of nCmP was weighed in a glass tube. The tube was tapped 200 times to ensure efficient packing of the nCmP and then the volume occupied by the particles was measured using digital calipers. The density was determined by the following equation:

$$\rho = \frac{m}{V}$$

where ρ is the tapped density of the nCmP, m is the nCmP mass, and V is the nCmP volume determined by measuring the height of the particles in a tube with a known diameter (5 mm). The theoretical MMAD ($MMAD_T$) of the nCmP was calculated using the following equation:

$$MMAD_T = d\sqrt{\frac{\rho}{\rho^*}}$$

where d is the geometric diameter of the nCmP determined by ImageJ, ρ is the tapped density, and $\rho^* = 1\ g/cm^3$ (reference density of solid polymer).

2.2.13 *In Vitro* Cytotoxicity of TAC nCmP—The *in vitro* cytotoxicity of TAC nCmP as well as free TAC was evaluated using the resazurin viability assay. A549 human adenocarcinoma alveolar epithelial cells were used as *in vitro* model to evaluate the effect of various TAC nCmP concentrations at different time intervals on their viability. A549 cells were maintained in DMEM supplemented with 10% (v/v) fetal bovine serum, 100 U/ml penicillin, 100 μg/ml streptomycin, Fungizone® (0.5 μg amphotericin, B, 0.41 μg/mL sodium deoxycholate), and 1 mM sodium pyruvate at 37°C in 5% CO_2. The cells were trypsinized and plated at density 5×10^4 cells/ml (100 μl/well) in flat-bottomed 96-well

plates and incubated overnight. After 24 hours, the A549 cells were exposed to various concentrations of free TAC and TAC nCmP (0.00001 to 10 μM) for 48 and 72 hours. After exposure, 20 μl of resazurin solution (60 μM) was added to each well and the plate was incubated for 3 hours, allowing the viable cells to convert resazurin to resorufin, and the fluorescence intensity of the resorufin produced by viable cells was detected at 520 nm (excitation) and 590 nm (emission) using a Cytation 3 plate reader (BioTek, Winooski, VT). The wells containing complete medium and resazurin, without cells, were used as the background measurement and wells containing cells and resazurin, without particles, served as the positive control. The relative viability of each sample was calculated by:

$$\text{Relative Viability} = \frac{\text{Fluorescence Intensity of Sample}}{\text{Fluorescence Intensity of Control}} \times 100\%$$

2.2.14 Statistical Analysis—All measurements were performed in at least triplicate. Values are given in the form of means ± SD. The statistical significance of the results was determined using Student's t-tests where a p-value of < 0.05 was considered statistically significant.

3. RESULTS AND DISCUSSION

3.1 Characterization of Ac-Dex

Ac-Dex exhibited 71.5% cyclic acetal coverage and 79.2% total conversion of -OH groups. An increase in CAC is known to decrease the drug release rate due to slower degradation of Ac-Dex (16, 17). A high total acetal coverage (higher than 75% according to our research) is necessary to stabilize the PVA coating of nanoparticles, which ensures small particles size and narrow size distribution. Therefore, NMR confirmed successful synthesis of Ac-Dex.

3.2 Characterization of Nanoparticles

3.2.1 NP Size, Distribution, and Surface Charge—The tacrolimus-loaded nanoparticles (TAC NP) shown in Figure 2A, appear as uniform spheres with smooth surface morphology. The apparent sintering evident in the SEM micrographs is likely an artifact of the PVA present on the NP and particle drying process prior to imaging. NP size, size distribution (polydispersity index, PDI), and zeta potential are shown in Table 1. The resulting sizes of the NP analyzed via DLS (approximately 200 nm) were larger than those observed from SEM micrographs and ImageJ analysis (approximately 100 nm) due to shrinking of the particles during drying and/or sputter coating and agglomeration of particles during resuspension into aqueous solutions (37, 38). The TAC NP exhibited desirable size (less than 200 nm) with narrow size distribution to potentially allow for mucus penetration and pulmonary epithelial targeting. The surface charge of the NP system was slightly negative, which is suitable to reduce interactions with negatively charged mucin fibers, potentially enhancing the particle permeation through the mucus barrier (38).

3.2.2 TAC Loading and In Vitro Release—TAC was successfully encapsulated into the TAC NP. 70.4% of the initially loaded TAC was effectively encapsulated within the NP prepared using emulsion solvent evaporation of Ac-Dex and drug in PVA solution. The high

encapsulation efficacy of the drug is due to the low solubility of TAC in the aqueous spinning solution.

Results of the *in vitro* release of TAC NP at physiological pH and temperature are reported in Figure 3 as the percentage of drug released over time. The TAC NP system displayed a sustained release of 40% of its payload after 12 hours, in which 30% of TAC was released in the first 6 hours and 10% was released in the next 6 hours. Previous research showed that similar Ac-Dex NP exhibited a maximum of degradation at 6 hours and negligible degradation after that (18). Based on these results, the TAC release profiles in this study can likely be explained as follows: the first release stage (up to 6 hours) corresponds to Ac-Dex degradation as well as nanoparticle dissociation, whereas after 6 hours the rate of TAC release is controlled by drugs passively diffusing out of the dissociated matrix of nanoparticles following the partial degradation of Ac-Dex. This two-stage release profile of Ac-Dex based particles matches that of other drug-loaded Ac-Dex nanoparticle systems in our group and other previous studies (36).

3.3 Nanocomposite Microparticle Characterization

3.3.1 nCmP Morphology, Size, and Size Distribution—TAC nCmP displayed a wrinkled and raisin-like surface with visibly encapsulated NP as seen in Figures 2B and 2C. The corrugated surface of the nCmP reduces their contact area, which helps to prevent the particles from aggregating upon aerosolization, thus improving aerosol performance and dispersion of the NP from the dry powder nCmP formulation. The cause of the raisin-like morphology of the nCmP may be attributed to the early formation of nanoparticle shells in droplets during spray drying. The formation of nanoparticle shells during spray drying determines the geometric size of nCmP. As the drying proceeds, the remaining water keeps evaporating from the droplet center, resulting in hollow particles that tend to shrink (39, 40). The number average geometric diameter of the TAC nCmP system was 2.13 ± 0.52 μm, as determined by ImageJ analysis.

3.3.2 Karl Fischer Titration—The residual water content of TAC nCmP was approximately 8 weight % (Table 2), which is acceptable in this dry powder formulation. Water in inhalable dry powders can significantly reduce their dispersion properties during aerosolization due to the interparticulate capillary forces acting at the solid–solid interface between particles (41) and the presence of water is also responsible for the instability of the powders during storage (42). Correspondingly, low water content in inhalable dry powders is highly favorable for efficient dry powder aerosolization and effective particle delivery (41, 43).

3.3.3 Differential Scanning Calorimetry—Figure 4 shows DSC thermograms of the raw materials used in particle preparation and the final drug-loaded nCmP. Raw Ac-Dex, TAC, and mannitol displayed endothermic main phase transition peaks (T_m) near 170, 135, and 167 °C, respectively, which are in accordance with previously reported values (44, 45). The TAC nCmP system exhibited a main phase transition peak (T_m) near 142 °C, corresponding to the melting of mannitol (see Figure S1). This melting point was lower than those of raw mannitol, indicating an increase in the amorphous state of these raw materials

in nCmP. No glass transitions or other phase transitions were evident under 120 °C, which indicated that all the materials are stable during manufacturing and storage conditions.

3.3.4 Powder X-ray Diffraction (PXRD)—X-ray diffraction diffractograms of the raw materials and TAC nCmP are shown in Figure 5. Strong peaks were present for raw TAC and mannitol powders. These strong peaks indicate that the raw materials were in their crystalline forms prior to spray drying, which is in accordance with previous studies (44, 45). No strong peaks were present for raw Ac-Dex, indicating that it is non-crystalline. The non-crystallinity of Ac-Dex is quite different from commercialized polymers such as PLGA, which exhibits strong XRD characterization peaks (46–48). The absence of diffraction peaks in Ac-Dex is likely because the Ac-Dex was collected by rapid precipitation in water. XRD patterns of TAC nCmP displayed the absence of any diffraction peaks of raw TAC, suggesting amorphization of raw TAC in the particle matrix, which is suitable for the improvement of tacrolimus solubility. Also, the peaks characterizing mannitol were significantly reduced, indicating that mannitol is reduced to its amorphous state in the nCmP. The results obtained from the XRD diffractograms confirmed those from DSC thermograms, where raw TAC and mannitol were converted into more amorphous forms during the nCmP manufacturing process.

3.3.5 Drug and Nanoparticle (NP) Loading in nCmP—UPLC was used to determine the amount of TAC loading in the nCmP and this data was used to calculate the resulting NP loading and NP encapsulation efficacy (EE) in the nCmP formulation as seen in Tables 1 and 2. The TAC nCmP showed high NP loading (> 45%), and very high NP EE (> 90%). The high drug loading in the nCmP formulation (approximately 3 mg of TAC per mg of nCmP) is favorable in order to reduce the amount of particles administrated to achieve a target therapeutic effect in the lungs and reduce the total particle load delivered.

3.3.6 Nanoparticle Redispersion from nCmP—The properties of NP redispersed from nCmP in water were evaluated using DLS (Table 1). The size and PDI of the redispersed NP exhibited slight increases after redispersion from nCmP, which is likely a result of agglomeration that occurred during the spray drying process. The NP surface charge remained slightly negative. These parameters were all within the desirable ranges for effective penetration of NP through the mucus barrier, demonstrating the favorable properties of nanoparticles remain intact after spray drying.

3.3.7 In Vitro Aerosol Dispersion Performance Using Next Generation Impactor (NGI)—*In vitro* aerosol dispersion performance properties of the nCmP were evaluated using a Next Generation Impactor™ coupled with a human DPI device (Figure 6 and Table 3). The results indicated that the formulated nCmP aerosol properties are favorable for efficient dry powder aerosolization and effective pulmonary delivery. The experimental mass mean aerodynamic diameter ($MMAD_E$) value of TAC-nCmP was 3.57 μm, while the geometric standard deviation (GSD) value was 1.78 μm. The $MMAD_E$ value is within the range of 1 – 5 μm that is required for predominant deposition of nCmP into the deep lung regions (49), which would be desirable for the delivery of TAC to the periphery of the lungs. The GSD values were within the range of those previously reported and the

respirable fraction (RF), fine particle fraction (FPF), and emitted dose (ED) values were all higher than reports from similar systems (34, 49, 50). In clinical research, PAH patients are treated with TAC with a target blood level of 1.5 – 5 ng/mL (51–53). The present nCmP system is expected to achieve a therapeutic effect using a low amount of TAC through its improved delivery efficacy over current systemic methods. As seen in Figure 6, 32.7 % of TAC nCmP deposited on stages 4 – 7 and it is predicted that these particles will deposit in the deep lung alveolar region due to diffusion mechanisms of deposition (54). Subsequently, 45.3% of nCmP deposited on stages 3 – 4 and are thus predicted to deposit in the lungs by sedimentation due to gravitational settling (21, 55, 56). Overall, the nCmP exhibited desirable aerosol dispersion characteristics allowing them to deposit in deep lung regions for effective drug delivery of TAC.

3.3.8 Analysis of nCmP Density and Theoretical Aerodynamic Diameter—The density of the particles was determined via tapped density measurements. The TAC nCmP exhibited a low density of 0.138 ± 0.001 g/cm^3 compared with the raw materials (1.5 g/cm^3), which can be attributed to the raisin-like surface morphology and hollow structure of the nCmP. The theoretical MMAD calculated with the geometric diameter and tapped density was 0.79 μm, which was lower than the experimental result (3.57 μm). The lower $MMAD_T$ in comparison to $MMAD_E$ can be attributed to nCmP agglomeration during aerosolization, which increased the geometric size (and thus aerodynamic diameter) of the dry powder formulation.

3.3.9 In Vitro Cytotoxicity of TAC nCmP Microparticles—To evaluate the response of pulmonary cells to particles, *in vitro* cytotoxicity analysis of TAC nCmP as well as free TAC against A549 cells was evaluated. For free TAC the relative viability of the A549 cells remains constant for increasing drug concentrations at 48 and 72 hours, demonstrating that TAC is non-toxic to lung cells up to 10 μM (Figure 7 (a)). TAC nCmP did not cause any significant cytotoxic effects at various TAC concentrations (0.00001 – 10 μM) and there was no significant decrease in the viability of A549 cells between 48 and 72 hours (Figure 7 (b)). Thus, TAC nCmP was not cytotoxic and could be used for the treatment of PAH, hence minimizing the potential negative side effects.

4. CONCLUSIONS

Tacrolimus was successfully encapsulated in Ac-Dex nanoparticles with a high encapsulation efficacy. The drug-loaded nanoparticles were 200 nm, smooth spheres with narrow size distribution and slightly negative surface charge, which is desirable to overcome the mucus barrier in the lung. These favorable properties were maintained during the nCmP manufacturing process as shown in redispersion testing. The nCmP systems were 2 μm, raisin-like spheres with observable nanoparticles present on their surface. The water content of the nCmP systems was relatively low, which can enable efficient dry powder aerosolization and particle delivery. None of the raw materials underwent degradation during nCmP manufacturing, indicating the stability of the therapeutics during formation. No crystalline structures of TAC was observed in the nCmP, which confirmed that the drug in the nCmP were in their amorphous form. *In vitro* aerosol performance testing demonstrated desirable aerosol dispersion characteristics of nCmP, allowing them to deposit in deep lung

regions for drug delivery. There was no significant effect in the viability of A549 cells, which confirmed the non-cytotoxic effect of TAC nCmP.

This nCmP system exhibits promising application in pulmonary TAC delivery for the treatment of PAH due to its novel features including targeted pulmonary delivery, improved solubility of tacrolimus, potential of permeation through mucus barrier, and of controlled drug release. In contrast to other delivery methods, this dry powder formulation also provides more convenient administration, more flexible storage conditions, and lower risk of contamination in the device.

Supplementary Material

Refer to Web version on PubMed Central for supplementary material.

Acknowledgments

The authors gratefully acknowledge financial support from an Institutional Development Award (IDeA) from the National Institute of General Medical Sciences of the National Institutes of Health under grant number P20GM103430. The content is solely the responsibility of the authors and does not necessarily represent the official views of the National Institutes of Health. This material is based upon work conducted at a Rhode Island NSF EPSCoR research facility, supported in part by the National Science Foundation EPSCoR Cooperative Agreement #EPS-1004057. In addition, this material is based in part upon work supported by the National Science Foundation under grant number #1508868. Any opinions, findings, and conclusions or recommendations expressed in this material are those of the authors and do not necessarily reflect the view of the National Science Foundation. Finally, the authors thank RI-INBRE for UPLC access and RIN2 for SEM, DLS, PXRD, and DSC access.

REFERENCES

1. Badiani B, Messori A. Targeted Treatments for Pulmonary Arterial Hypertension: Interpreting Outcomes by Network Meta-analysis. Heart, lung & circulation. 2016; 25(1):46–52.
2. Chin KM, Rubin LJ. Pulmonary Arterial Hypertension. Journal of the American College of Cardiology. 2008; 51(16):1527–1538. [PubMed: 18420094]
3. Montani D, Chaumais M-C, Guignabert C, Günther S, Girerd B, Jaïs X, Algalarrondo V, Price LC, Savale L, Sitbon O, Simonneau G, Humbert M. Targeted therapies in pulmonary arterial hypertension. Pharmacology & Therapeutics. 2014; 141(2):172–191. [PubMed: 24134901]
4. Spiekerkoetter E, Tian X, Cai J, Hopper RK, Sudheendra D, Li CG, El-Bizri N, Sawada H, Haghighat R, Chan R, Haghighat L, de Jesus Perez V, Wang L, Reddy S, Zhao M, Bernstein D, Solow-Cordero DE, Beachy PA, Wandless TJ, ten Dijke P, Rabinovitch M. FK506 activates BMPR2, rescues endothelial dysfunction, and reverses pulmonary hypertension. The Journal of Clinical Investigation. 2013; 123(8):3600–3613. [PubMed: 23867624]
5. Evans JDW, Girerd B, Montani D, Wang X-J, Galiè N, Austin ED, Elliott G, Asano K, Grünig E, Yan Y, Jing Z-C, Manes A, Palazzini M, Wheeler LA, Nakayama I, Satoh T, Eichstaedt C, Hinderhofer K, Wolf M, Rosenzweig EB, Chung WK, Soubrier F, Simonneau G, Sitbon O, Gräf S, Kaptoge S, Di Angelantonio E, Humbert M, Morrell NW. BMPR2 mutations and survival in pulmonary arterial hypertension: an individual participant data meta-analysis. The Lancet Respiratory Medicine.
6. Soubrier F, Chung WK, Machado R, Grünig E, Aldred M, Geraci M, Loyd JE, Elliott CG, Trembath RC, Newman JH, Humbert M. Genetics and Genomics of Pulmonary Arterial Hypertension. Journal of the American College of Cardiology. 2013; 62(25, Supplement):D13–D21. [PubMed: 24355637]
7. Rubin LJ, Galiè N. Pulmonary arterial hypertension: a look to the future. Journal of the American College of Cardiology. 2004; 43(12, Supplement):S89–S90.
8. West J, Austin E, Fessel JP, Loyd J, Hamid R. Rescuing the BMPR2 signaling axis in pulmonary arterial hypertension. Drug Discovery Today. 2014; 19(8):1241–1245. [PubMed: 24794464]

9. Trulock EP, Edwards LB, Taylor DO, Boucek MM, Keck BM, Hertz MI. Registry of the International Society for Heart and Lung Transplantation: Twenty-third Official Adult Lung and Heart–Lung Transplantation Report—2006. The Journal of Heart and Lung Transplantation. 25(8): 880–892. [PubMed: 16890108]

10. Schrepfer S, Deuse T, Reichenspurner H, Hoffmann J, Haddad M, Fink J, Fischbein MP, Robbins RC, Pelletier MP. Effect of inhaled tacrolimus on cellular and humoral rejection to prevent posttransplant obliterative airway disease. American journal of transplantation : official journal of the American Society of Transplantation and the American Society of Transplant Surgeons. 2007; 7(7):1733–1742.

11. Shivshankar P, Payan H, Calhoun C, Levine S, Williams RO, Jagirdar J, Peters JI, Jourdan Le Saux C. Inhaled tacrolimus modulates pulmonary fibrosis without promoting inflammation in bleomycin-injured mice. Journal of Drug Delivery Science and Technology. 2014; 24(5):469–477.

12. Vicari-Christensen M, Repper S, Basile S, Young D. Tacrolimus: review of pharmacokinetics, pharmacodynamics, and pharmacogenetics to facilitate practitioners' understanding and offer strategies for educating patients and promoting adherence. Prog Transplant. 2009; 19(3):277–284. [PubMed: 19813492]

13. Xu W, Ling P, Zhang T. Toward immunosuppressive effects on liver transplantation in rat model: Tacrolimus loaded poly(ethylene glycol)-poly(d,l-lactide) nanoparticle with longer survival time. International Journal of Pharmaceutics. 2014; 460(1–2):173–180. [PubMed: 24172796]

14. Arima H, Yunomae K, Miyake K, Irie T, Hirayama F, Uekama K. Comparative studies of the enhancing effects of cyclodextrins on the solubility and oral bioavailability of tacrolimus in rats. J Pharm Sci. 2001; 90(6):690–701. [PubMed: 11357172]

15. Kur F, Reichenspurner H, Meiser BM, Welz A, Furst H, Muller C, Vogelmeier C, Schwaiblmaier M, Briegel J, Reichart B. Tacrolimus (FK506) as primary immunosuppressant after lung transplantation. The Thoracic and cardiovascular surgeon. 1999; 47(3):174–178. [PubMed: 10443520]

16. Broaders KE, Cohen JA, Beaudette TT, Bachelder EM, Fréchet JMJ. Acetalated dextran is a chemically and biologically tunable material for particulate immunotherapy. Proceedings of the National Academy of Sciences. 2009; 106(14):5497–5502.

17. Bachelder EM, Beaudette TT, Broaders KE, Dashe J, Fréchet JMJ. Acetal-Derivatized Dextran: An Acid-Responsive Biodegradable Material for Therapeutic Applications. Journal of the American Chemical Society. 2008; 130(32):10494–10495. [PubMed: 18630909]

18. Kauffman KJ, Kanthamneni N, Meenach SA, Pierson BC, Bachelder EM, Ainslie KM. Optimization of rapamycin-loaded acetalated dextran microparticles for immunosuppression. International Journal of Pharmaceutics. 2012; 422(1–2):356–363. [PubMed: 22037446]

19. Coelho JF, Ferreira PC, Alves P, Cordeiro R, Fonseca AC, Góis JR, Gil MH. Drug delivery systems: Advanced technologies potentially applicable in personalized treatments. The EPMA Journal. 2010; 1(1):164–209. [PubMed: 23199049]

20. Park CWM, Heidi M. Hayes, Don Pulmonary inhalation aerosols for targeted antibiotics drug delivery. European Pharmaceutical Review. 2011; 1

21. Hickey, AJ.; Mansour, Heidi M. Delivery of Drugs by the Pulmonary Route. In: A, T.; Florence, JS., editors. Modern Pharmaceutics: Applications and Advances. New York, NY: Informa Healthcare; 2009. p. 191-219.

22. Hayes D Jr, Zwischenberger JB, Mansour HM. Aerosolized tacrolimus: a case report in a lung transplant recipient. Transplantation proceedings. 2010; 42(9):3876–3879. [PubMed: 21094875]

23. Patton JS, Byron PR. Inhaling medicines: delivering drugs to the body through the lungs. Nat Rev Drug Discov. 2007; 6(1):67–74. [PubMed: 17195033]

24. Yang X-F, Xu Y, Qu D-S, Li H-Y. The influence of amino acids on aztreonam spray-dried powders for inhalation. Asian Journal of Pharmaceutical Sciences. 2015; 10(6):541–548.

25. Wu L, Miao X, Shan Z, Huang Y, Li L, Pan X, Yao Q, Li G, Wu C. Studies on the spray dried lactose as carrier for dry powder inhalation. Asian Journal of Pharmaceutical Sciences. 2014; 9(6): 336–341.

26. Stegemann S, Kopp S, Borchard G, Shah VP, Senel S, Dubey R, Urbanetz N, Cittero M, Schoubben A, Hippchen C, Cade D, Fuglsang A, Morais J, Borgstrom L, Farshi F, Seyfang KH,

Hermann R, van de Putte A, Klebovich I, Hincal A. Developing and advancing dry powder inhalation towards enhanced therapeutics. European journal of pharmaceutical sciences : official journal of the European Federation for Pharmaceutical Sciences. 2013; 48(1–2):181–194. [PubMed: 23142635]

27. Ong HX, Traini D, Ballerin G, Morgan L, Buddle L, Scalia S, Young PM. Combined Inhaled Salbutamol and Mannitol Therapy for Mucus Hyper-secretion in Pulmonary Diseases. Aaps J. 2014; 16(2):269–280. [PubMed: 24431080]
28. Kaialy W, Larhrib H, Martin G, Nokhodchi A. The Effect of Engineered Mannitol-Lactose Mixture on Dry Powder Inhaler Performance. Pharm Res. 2012; 29(8):2139–2156. [PubMed: 22477070]
29. Kramek-Romanowska K, Odziomek M, Sosnowski TR, Gradoń L. Effects of Process Variables on the Properties of Spray-Dried Mannitol and Mannitol/Disodium Cromoglycate Powders Suitable for Drug Delivery by Inhalation. Industrial & Engineering Chemistry Research. 2011; 50(24): 13922–13931.
30. Littringer EM, Paus R, Mescher A, Schroettner H, Walzel P, Urbanetz NA. The morphology of spray dried mannitol particles — The vital importance of droplet size. Powder Technology. 2013; 239:162–174.
31. Guimarães TF, Lanchote AD, da Costa JS, Viçosa AL, de Freitas LAP. A multivariate approach applied to quality on particle engineering of spray-dried mannitol. Advanced Powder Technology. 2015; 26(4):1094–1101.
32. Littringer EM, Mescher A, Schroettner H, Achelis L, Walzel P, Urbanetz NA. Spray dried mannitol carrier particles with tailored surface properties – The influence of carrier surface roughness and shape. European Journal of Pharmaceutics and Biopharmaceutics. 2012; 82(1):194–204. [PubMed: 22595133]
33. Jensen DMK, Cun D, Maltesen MJ, Frokjaer S, Nielsen HM, Foged C. Spray drying of siRNA-containing PLGA nanoparticles intended for inhalation. Journal of Controlled Release. 2010; 142(1):138–145. [PubMed: 19840823]
34. Meenach SA, Anderson KW, Zach Hilt J, McGarry RC, Mansour HM. Characterization and aerosol dispersion performance of advanced spray-dried chemotherapeutic PEGylated phospholipid particles for dry powder inhalation delivery in lung cancer. European Journal of Pharmaceutical Sciences. 2013; 49(4):699–711. [PubMed: 23707466]
35. W F. The ARLA Respiratory Deposition Calculator. 2008
36. Meenach SA, Kim YJ, Kauffman KJ, Kanthamneni N, Bachelder EM, Ainslie KM. Synthesis, Optimization, and Characterization of Camptothecin-Loaded Acetalated Dextran Porous Microparticles for Pulmonary Delivery. Molecular Pharmaceutics. 2012; 9(2):290–298. [PubMed: 22149217]
37. Bootz A, Vogel V, Schubert D, Kreuter J. Comparison of scanning electron microscopy, dynamic light scattering and analytical ultracentrifugation for the sizing of poly(butyl cyanoacrylate) nanoparticles. European Journal of Pharmaceutics and Biopharmaceutics. 2004; 57(2):369–375. [PubMed: 15018998]
38. Householder KT, DiPerna DM, Chung EP, Wohlleb GM, Dhruv HD, Berens ME, Sirianni RW. Intravenous delivery of camptothecin-loaded PLGA nanoparticles for the treatment of intracranial glioma. Int J Pharm. 2015; 479(2):374–380. [PubMed: 25562639]
39. You Y, Zhao M, Liu G, Tang X. Physical characteristics and aerosolization performance of insulin dry powders for inhalation prepared by a spray drying method. The Journal of pharmacy and pharmacology. 2007; 59(7):927–934. [PubMed: 17637186]
40. Vehring R. Pharmaceutical Particle Engineering via Spray Drying. Pharm Res. 2008; 25(5):999–1022. [PubMed: 18040761]
41. Hickey AJ, Mansour HM, Telko MJ, Xu Z, Smyth HD, Mulder T, McLean R, Langridge J, Papadopoulos D. Physical characterization of component particles included in dry powder inhalers. I. Strategy review and static characteristics. J Pharm Sci. 2007; 96(5):1282–1301. [PubMed: 17455324]
42. Wu X, Zhang W, Hayes D, Mansour HM. Physicochemical characterization and aerosol dispersion performance of organic solution advanced spray-dried cyclosporine A multifunctional particles for

dry powder inhalation aerosol delivery. International Journal of Nanomedicine. 2013; 8:1269–1283. [PubMed: 23569375]

43. Nora YKC, Hak-Kim Chan. The Role of Particle Properties in Pharmaceutical Powder Inhalation Formulations. Journal of Aerosol Medicine. 2002; 15(3):325–330. [PubMed: 12396421]
44. Kaialy W, Nokhodchi A. Dry powder inhalers: Physicochemical and aerosolization properties of several size-fractions of a promising alterative carrier, freeze-dried mannitol. European Journal of Pharmaceutical Sciences. 2015; 68:56–67. [PubMed: 25497318]
45. Wu X, Hayes D, Zwischenberger JB, Kuhn RJ, Mansour HM. Design and physicochemical characterization of advanced spray-dried tacrolimus multifunctional particles for inhalation. Drug Design, Development and Therapy. 2013; 7:59–72.
46. Mohammadi G, Valizadeh H, Barzegar-Jalali M, Lotfipour F, Adibkia K, Milani M, Azhdarzadeh M, Kiafar F, Nokhodchi A. Development of azithromycin–PLGA nanoparticles: Physicochemical characterization and antibacterial effect against Salmonella typhi. Colloids and Surfaces B: Biointerfaces. 2010; 80(1):34–39. [PubMed: 20558048]
47. Zhang Z, Xu L, Chen H, Li X. Rapamycin-loaded poly(ε-caprolactone)-poly(ethylene glycol)-poly(ε-caprolactone) nanoparticles: preparation, characterization and potential application in corneal transplantation. Journal of Pharmacy and Pharmacology. 2014; 66(4):557–563. [PubMed: 24635557]
48. Li X, Chang S, Du G, Li Y, Gong J, Yang M, Wei Z. Encapsulation of azithromycin into polymeric microspheres by reduced pressure-solvent evaporation method. International Journal of Pharmaceutics. 2012; 433(1–2):79–88. [PubMed: 22583850]
49. Meenach SA, Vogt FG, Anderson KW, Hilt JZ, McGarry RC, Mansour HM. Design, physicochemical characterization, and optimization of organic solution advanced spray-dried inhalable dipalmitoylphosphatidylcholine (DPPC) and dipalmitoylphosphatidylethanolamine poly(ethylene glycol) (DPPE-PEG) microparticles and nanoparticles for targeted respiratory nanomedicine delivery as dry powder inhalation aerosols. International Journal of Nanomedicine. 2013; 8:275–293. [PubMed: 23355776]
50. Ungaro F, De Rosa G, Miro A, Quaglia F, La Rotonda MI. Cyclodextrins in the production of large porous particles: Development of dry powders for the sustained release of insulin to the lungs. European Journal of Pharmaceutical Sciences. 2006; 28(5):423–432. [PubMed: 16806857]
51. Edda S. FK506 (Tacrolimus) in Pulmonary Arterial Hypertension (TransformPAH). 2012
52. Spiekerkoetter E, Sung YK, Sudheendra D, Bill M, Aldred MA, van de Veerdonk MC, Vonk Noordegraaf A, Long-Boyle J, Dash R, Yang PC, Lawrie A, Swift AJ, Rabinovitch M, Zamanian RT. Low-Dose FK506 (Tacrolimus) in End-Stage Pulmonary Arterial Hypertension. American journal of respiratory and critical care medicine. 2015; 192(2):254–257. [PubMed: 26177174]
53. Roham TZ, Yon S, Val S, Yuwen L, Janel L-B, Edda S. TrANsFoRM PAH: Phase II Study Of Safety And Efficacy Of FK-506 (Tacrolimus) In Pulmonary Arterial Hypertension. B64 MANAGEMENT OF PULMONARY HYPERTENSION: American Thoracic Society. 2013:A3275–A3275.
54. S S, H AJ. Drug properties affecting aerosol behavior. Respiratory Care. 2000; 45(6):652–666. [PubMed: 10894458]
55. Hickey, AJ.; Mansour, HM. Formulation challenges of powders for the delivery of small molecular weight molecules as aerosols. In: R, MJ.; H, J.; R, MS.; L, ME., editors. Modified-Release Drug Delivery Technology. New York: Informa Healthcare; 2008.
56. Edwards DA. The macrotransport of aerosol particles in the lung: Aerosol deposition phenomena. Journal of Aerosol Science. 1995; 26(2):293–317.

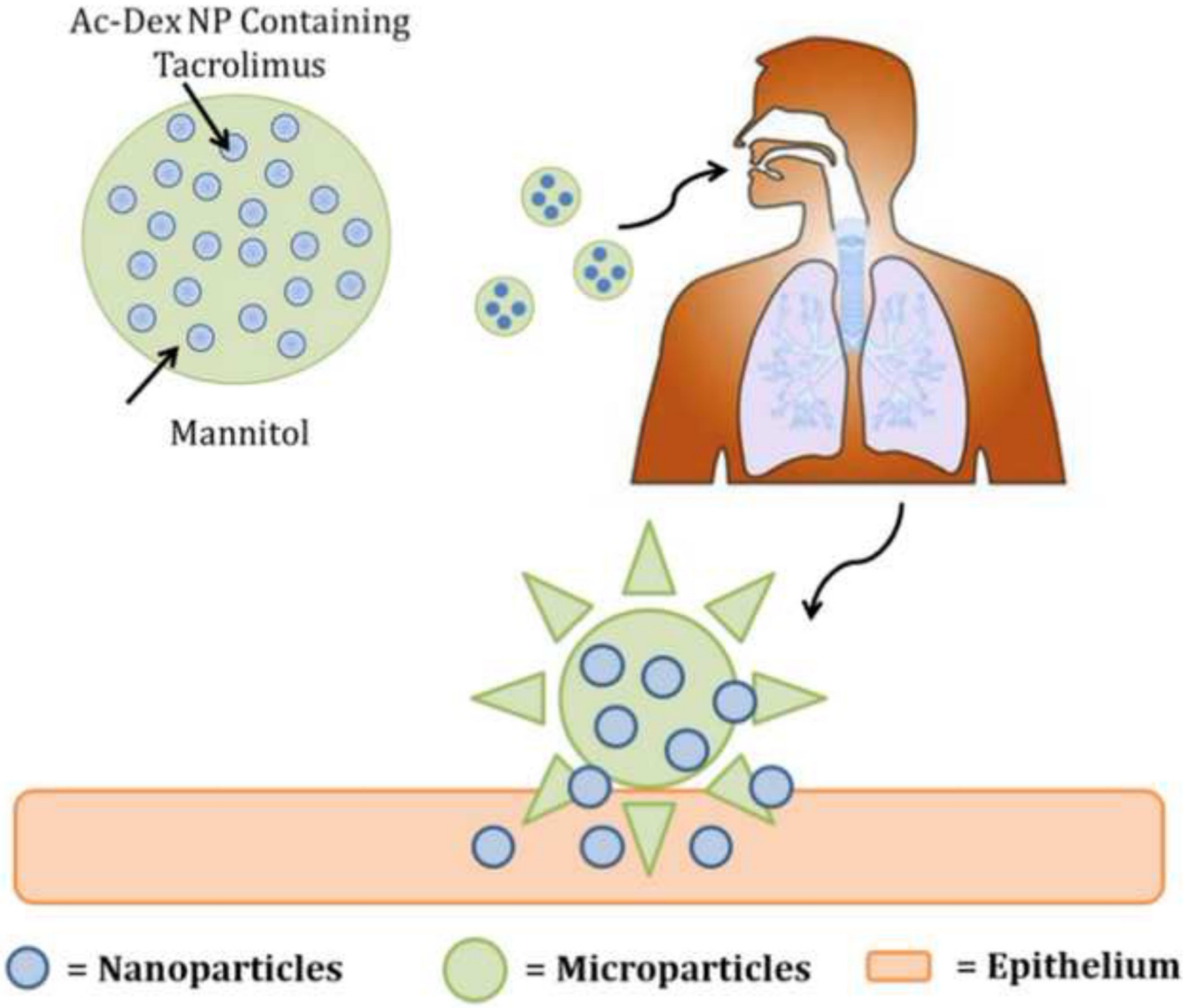

Figure 1.

Schematic of an aerosol nanoparticle microparticle (nCmP) system interacting with the pulmonary mucosa and epithelium. Once the nCmP impact the surface of the mucus coating the pulmonary epithelium they immediately degrade to release nanoparticles.

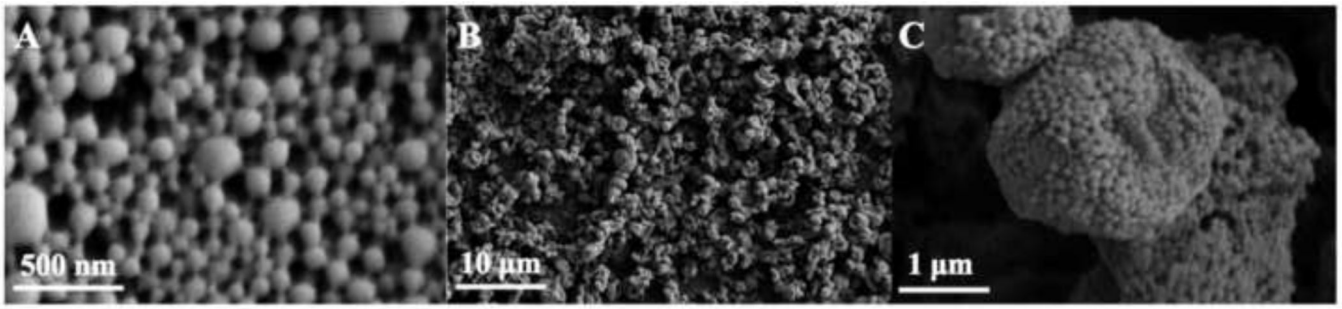

Figure 2.

Representative SEM micrographs of tacrolimus (TAC) nanoparticles (NP) and nanocomposite microparticles (nCmP) including: (A) tacrolimus-loaded nanoparticles (TAC NP), (B) tacrolimus-loaded nanocomposite microparticles (TAC nCmP), and (C) representative zoomed in image of TAC nCmP.

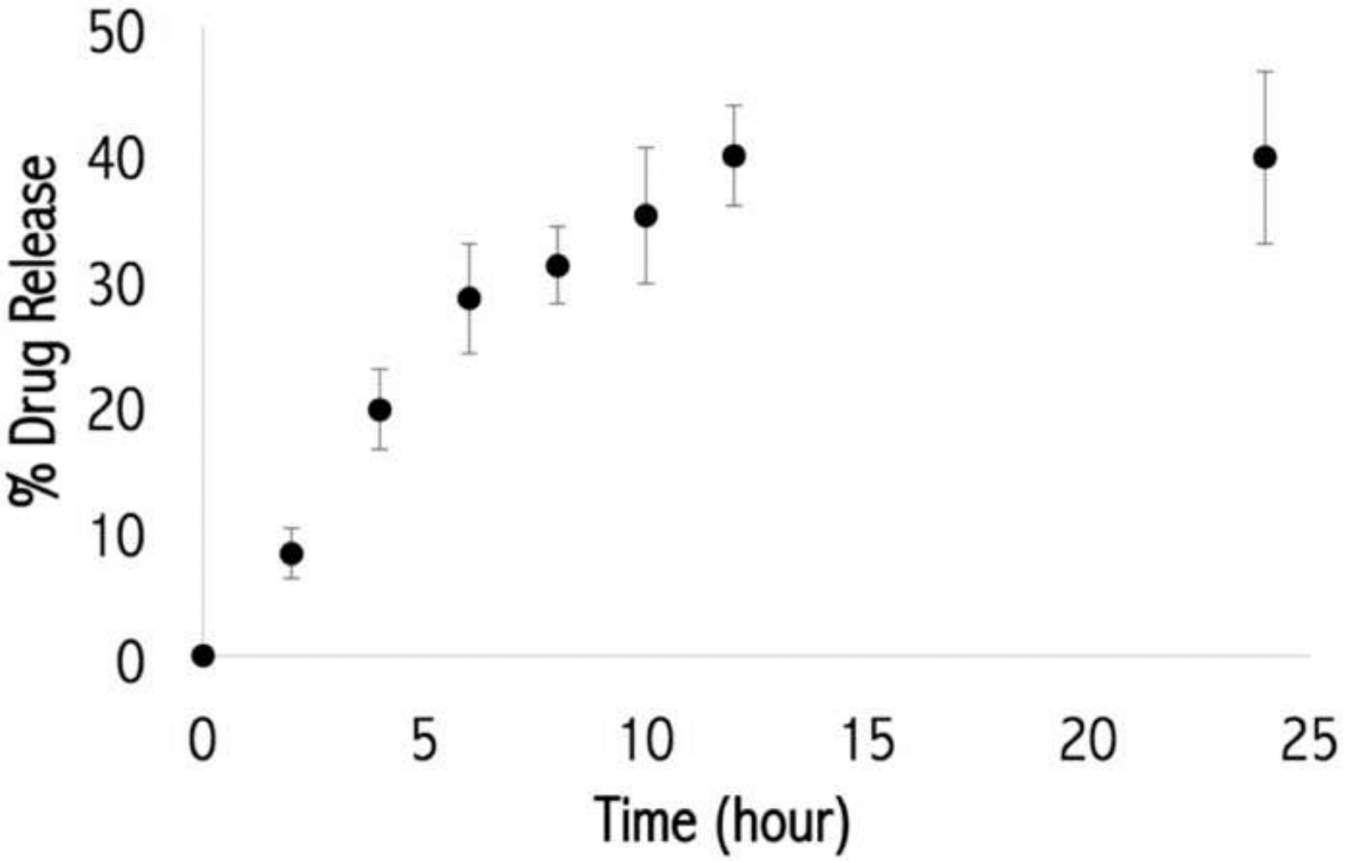

Figure 3.
In vitro drug release profile for tacrolimus (TAC) nanoparticle system.

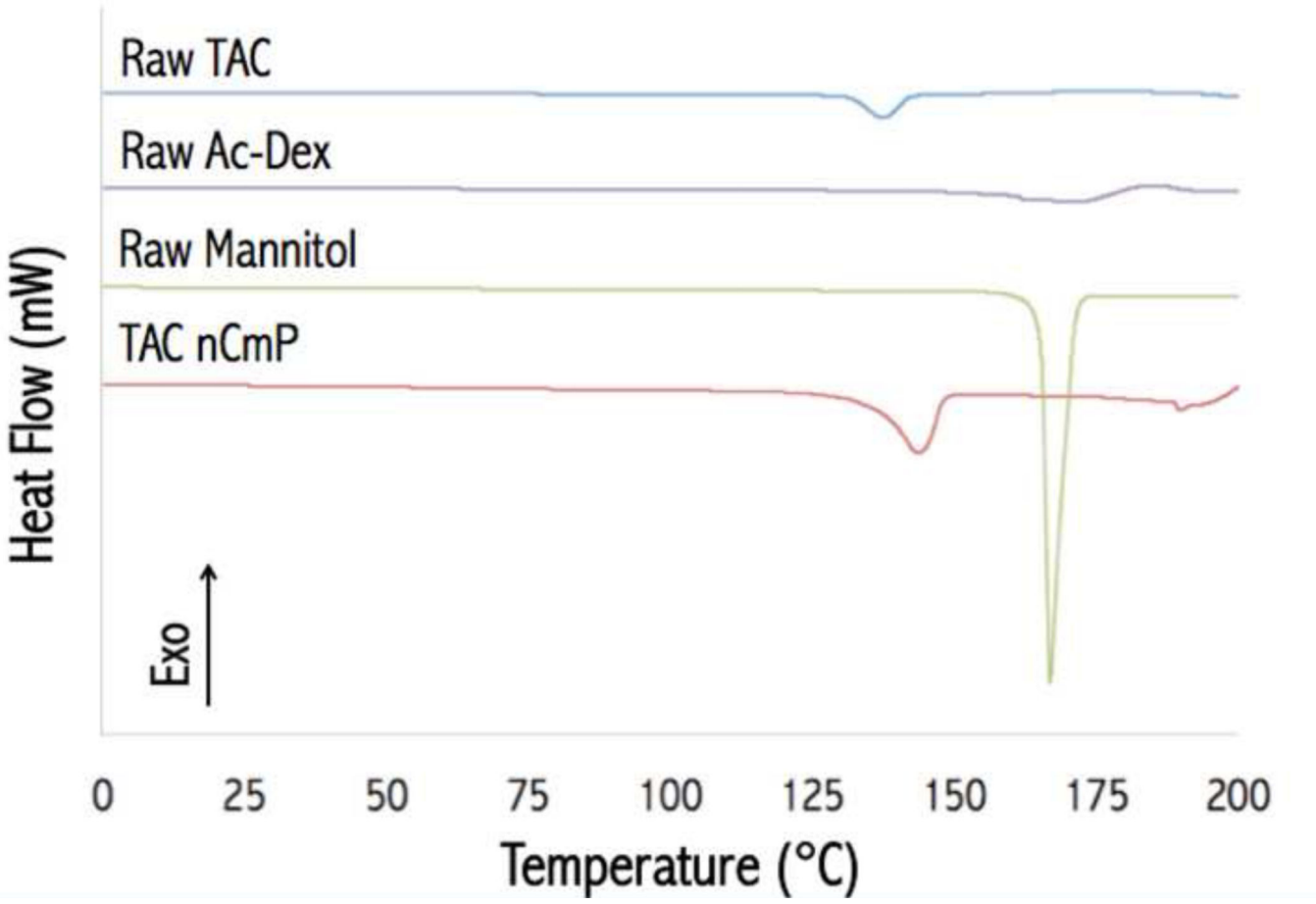

Figure 4.

Representative differential scanning calorimetry (DSC) thermograms of raw tacrolimus (TAC), raw acetalated dextran (Ac-Dex), raw mannitol, and formulated TAC nanocomposite microparticles (TAC nCmP).

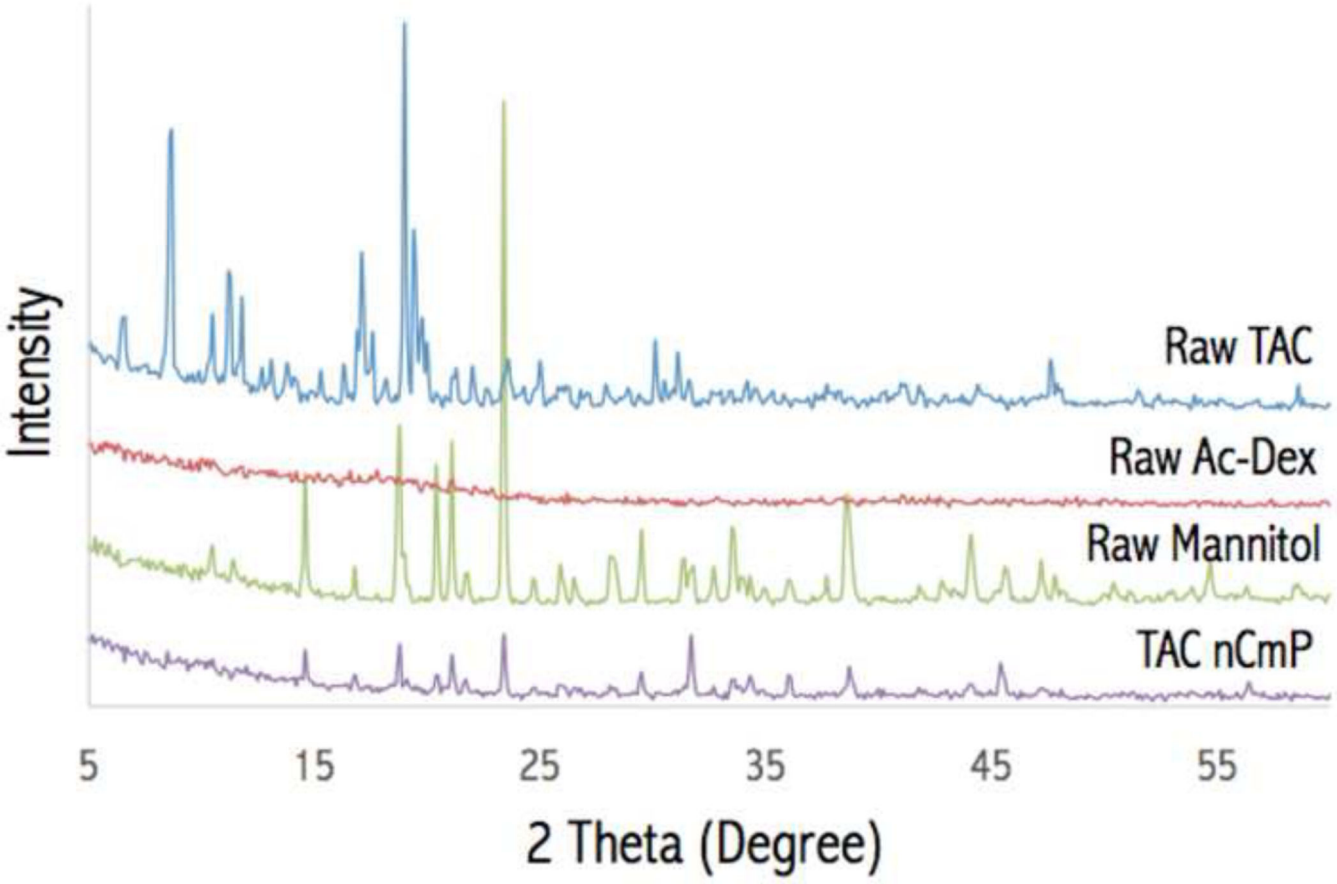

Figure 5.
Representative powder X-ray (PXRD) diffractograms of raw tacrolimus (TAC), raw acetalated dextran (Ac-Dex), raw mannitol, and formulated TAC nanocomposite microparticles (TAC nCmP).

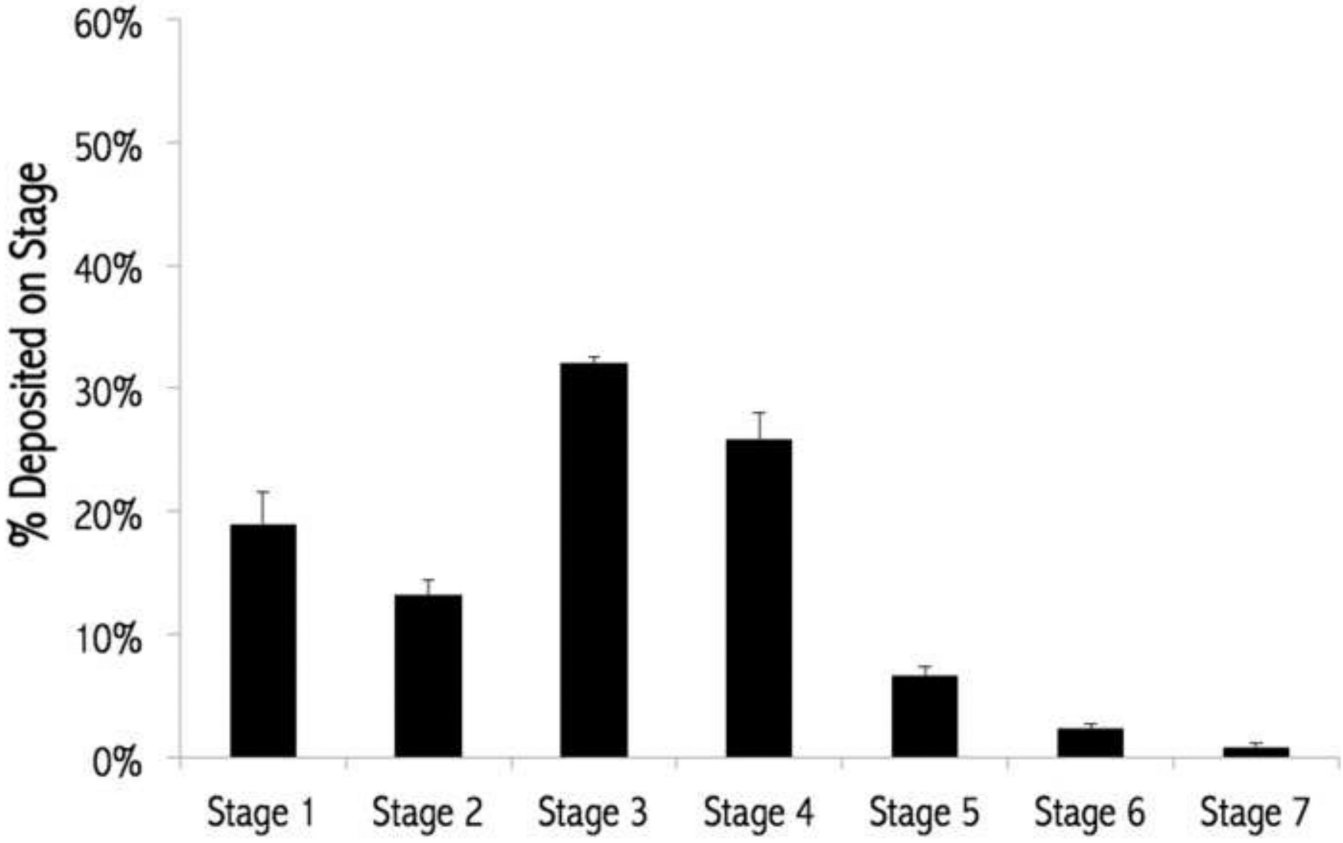

Figure 6.

Aerosol dispersion performance of tacrolimus nanocomposite microparticles (TAC nCmP) as % particles deposited on each stage of the Next Generation Impactor™ (NGI™). For Q = 60 L/min, the effective cutoff diameters (D_{50}) for each impaction stage are as follows: stage 1 (8.06 μm), stage 2 (4.46 μm), stage 3 (2.82 μm), stage 4 (1.66 μm), stage 5 (0.94 μm), stage 6 (0.55 μm), and stage 7 (0.34 μm) (n = 3, Average ± SD).

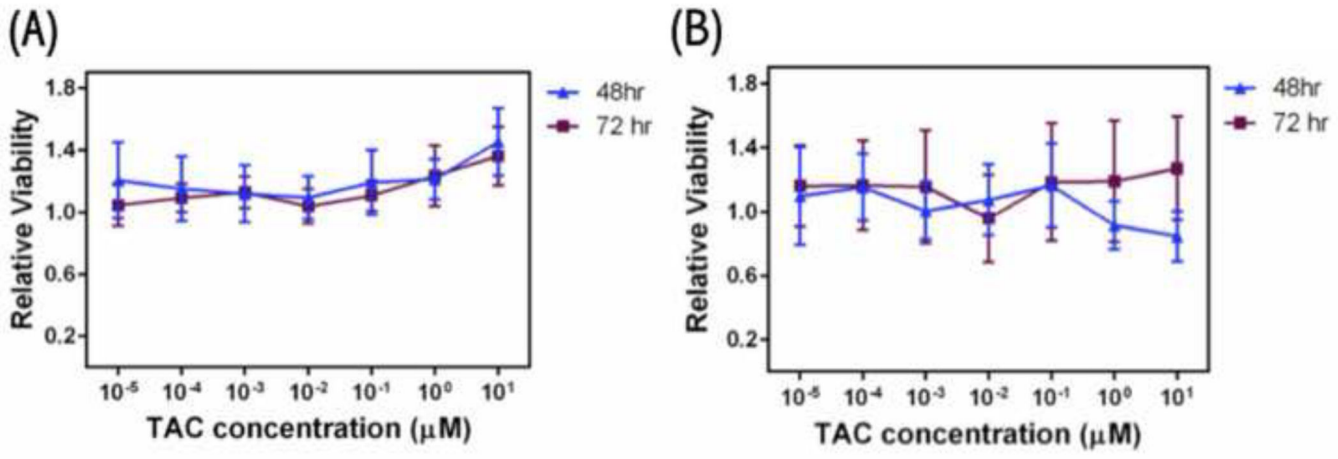

Figure 7.

A549 cell viability measured by resazurin assay after 48 h and 72 h exposure to (a) free TAC, and (b) TAC nanocomposite microparticles (ncmp) (n = 3, Average ± SD).

Table 1

Diameter (as measured by dynamic light scattering), polydispersity index (PDI), zeta potential (ζ), TAC loading, and encapsulation efficiency (EE) of tacrolimus-loaded nanoparticles before spray drying (TAC NP) and after spray drying and redispersion from nanocomposite microparticles (Redispersed TAC NP) (mean ± standard deviation, n = 3).

System	Diameter (nm)	PDI	ζ Potential (mV)	TAC Loading (mg drug/100mg NP)	EE (%)
TAC NP	199.7 ± 3.2	0.07 ± 0.00	−6.33 ± 1.27	7.04 ± 0.45	70.4 ± 4.4
Redispersed TAC NP	227.5 ± 6.3	0.16 ± 0.03	−9.42 ± 3.83	N/A	N/A

Table 2

Geometric diameter (as measured by SEM imaging and ImageJ analysis), water content, TAC loading, nanoparticle (NP) loading in nanocomposite microparticles (nCmP), and NP loading efficacy in nCmP (mean ± standard deviation, n = 3).

System	Geometric Diameter (μm)	Water Content (weight %)	Drug Loading (mg drug/100 mg nCmP)	NP Loading (%)	NP Loading Efficacy (%)
TAC nCmP	2.13 ± 0.52	7.99 ± 0.31	3.19 ± 0.31	45.29 ± 4.42	90.59 ± 8.85

Table 3

Tapped density analysis and *in vitro* aerosol dispersion performance properties for nanocomposite microparticles (TAC nCmP) including tapped density (ρ), theoretical mass median aerodynamic diameter ($MMAD_T$) from tapped density measurements, experimental mass median aerodynamic diameter ($MMAD_E$), geometric standard deviation (GSD), fine particle dose (FPD), fine particle fraction (FPF), respirable fraction (RF), and emitted dose (ED) for nCmP (mean ± standard deviation, n = 3).

System	ρ (g/cm^3)	$MMAD_T$ (μm)	$MMAD_E$ (μm)	GSD (μm)	FPF (%)	RF (%)	ED (%)
TAC nCmP	0.138 ± 0.001	0.79 ± 0.79	3.57 ± 0.17	1.78 ± 0.02	81.0 ± 2.6	67.6 ± 3.0	96.3 ± 1.37

Int J Pharm. Author manuscript; available in PMC 2017 October 15.